Facile Synthesis of Au-Nanoparticle/Polyoxometalate/Graphene Tricomponent Nanohybrids: An Enzyme-Free Electrochemical Biosensor for Hydrogen Peroxide

Rongji Liu, Shiwen Li, Xuelian Yu, Guangjin Zhang, Suojiang Zhang,* Jiannian Yao, Bineta Keita,* Louis Nadjo, and Linjie Zhi*

***A** green, facile, one-pot synthesis of well-defined Au NPs@POM–GNSs tricomponent nanohybrids is reported (POM stands for polyoxometalate and GNSs for graphene nanosheets). The synthesis is convenient, rapid and environmentally friendly. The POMs serve as both reducing, encapsulating molecules, and bridging molecules; this avoids the introduction of other organic toxic molecules. Characterization using transmission electron microscopy, X-ray diffraction, X-ray photoelectron spectroscopy, and Raman spectroscopy analysis is performed, and the structure of the prepared nanohybrids of Au NPs@POM–GNSs is verified. Most importantly, the amperometric measurements show the Au NPs@POM–GNSs nanohybrids have high catalytic activity with good sensitivity, good long-term stability, wide linear range, low detection limit, and fast response towards H_2O_2 detection for application as an enzyme-free biosensor. Transformation of the POMs during H_2O_2 detection does not affect the catalytic activities of the nanohybrids. Thus, the synergistic effect of Au NPs and GNSs in the nanohybrids leads to the enhanced catalytic property.*

1. Introduction

Since its discovery by Novoselov et al.,[1] graphene, with an atomically thin two-dimensional lattice of sp^2 carbon atoms packed into a dense honeycomb, and characterized as "the thinnest known material in the universe and the strongest ever measured", has received considerable attention due to its high surface area (around 2600 $m^2\ g^{-1}$),[2] high chemical

Dr. R. Liu, Dr. X. Yu, Prof. G. Zhang, Prof. S. Zhang
Key Laboratory of Green Process and Engineering
Beijing Key Laboratory of Ionic Liquids Clean Process
Institute of Process Engineering
Chinese Academy of Sciences
100190, Beijing, PR China
E-mail: zhanggj@home.ipe.ac.cn; sjzhang@home.ipe.ac.cn
Dr. R. Liu
Graduate University of Chinese Academy of Sciences
100049, Beijing, PR China
S. Li, Dr. B. Keita, Prof. L. Nadjo
Laboratoire de Chimie Physique
Equipe d'Electrochimie et de Photoélectrochimie
UMR 8000 CNRS, Université Paris-Sud 11, 91405 Orsay Cedex, France
E-mail: bineta.keita@u-psud.fr
Prof. J. Yao
Beijing National Laboratory for Molecular Science
Key Laboratory of Photochemistry
Institute of Chemistry
Chinese Academy of Sciences
100190, Beijing, PR China
Prof. L. Zhi
National Center for Nanoscience and Technology of China
Zhongguancun, Beiyitiao 11, 100190, Beijing, PR China

DOI: 10.1002/smll.201102298

NANO MICRO small

stability,[3] and unique electronic[4–6] and mechanical properties,[7] which ensure its potential applications in many fields, such as nanocomposites,[5,8] field-effect transistors,[9b,10] batteries,[11] solar cells,[12] supercapacitors,[2] nanoelectronics,[13] and ultrasensitive sensors.[14,15] In parallel, metal nanoparticles (NPs) have emerged as a new class of materials due to their unique electronic, optical, magnetic, and catalytic properties.[16] Thus, much effort has been made to decorate graphene nanosheets (GNSs) with various metal NPs, in order to produce novel nanohybrid materials with properties from two functional nanoscale materials combined, to achieve a wider range of applications.[17] For these purposes, a large variety of conditions and protocols were followed for synthesis of nanohybrid of metal NPs–GNSs, including, for example, microwave treatment,[18] sonochemical methods,[19] electrodeposition,[20] and chemical deposition.[21] Among these, chemical reduction holds the great advantage of low cost and bulk quantity production. However, as many of these approaches employ reductants, especially hydrazine, they are highly hazardous, use of which should be made with extreme care and minimized. Also the chemical processes are time-consuming and require high temperature. Thus, it is desirable to develop a simple, mild and effective route that provides well-dispersed metal NPs with good controllability and reproducibility without using hazardous organic molecules. Among the NPs, the attachment of Au NPs to GNSs is particularly promising for novel, highly efficient electrochemical cells and photoelectronic sensor devices. Thus, more and more attention has been aroused towards the development of both enzymatic[22–24] and enzyme-free[25,26] hybrid Au–GNS-based biosensors. In particular, enzyme-free biosensors have received more interest because they show promise in overcoming various drawbacks of enzymatic ones, including a complex structure that increases cost and poor long-term stability due to the inherent nature of enzymes. Hydrogen peroxide (H_2O_2) is not only a reactive oxygen species as an essential mediator[27] but also a by-product of many oxidative biological reactions, including those of glucose oxidase, cholesterol oxidase, uricase, alcohol oxidase, galactose oxidase, sarcosine oxidase, and L-amino-acid oxidase, etc. Thus it is important to develop a good biosensor for detection of H_2O_2 with high sensitivity, long stability, large detection range, and good selectivity. Various Au NP-based biosensors have been developed, however, to the best of our knowledge, only a few systems showed satisfactory properties regarding the above parameters. The attachement of Au NPs on GNSs may increase the electrocatalytic activities and thus improve the properties of the biosensors. Therefore, it is important to develop a facile method for preparation of Au NP–GNSs nanohybrids for enzyme-free biosensors of H_2O_2.

Recently, we developed a novel green method for decoration of Au, Pt, and Ag NPs on carbon nanotubes (CNTs) by using polyoxometalate (POMs) as the sole agent to build metal NPs@POM–CNTs tricomponent nanohybrids.[28] It has also been reported that POMs can act as an effective photocatalyst to reduce graphene oxide (GO) nanosheets under UV irradiation,[9] yielding reduced graphene oxide (RGO) with good electrical conductivity. POMs are early transition metal oxygen anionic clusters, which exhibit remarkably rich redox and photoelectrochemical properties, and thus show promising properties in photo-electrocatalysis.[29,30]

Herein, we report for the first time a facile approach to prepare nanohybrid Au NPs@POM–GNSs materials without the addition of other surface active agents. Specifically, the POM $H_3PW_{12}O_{40}$ (denoted as PW12 hereafter), with a typical Keggin structure, has been employed to serve as both a reducing and encapsulating molecule for the NPs and GNSs, as well as a bridging molecule. Our work represents a new type of tricomponent Au NPs@POM–GNSs heterostructure with several important benefits. The reaction can be performed at room temperature without any other organic templates and surfactants, which is beneficial for its electrocatalytic activities. Well dispersed and uniform Au NPs were decorated onto the GNSs. Encouragingly, such a nanohybrid offered a remarkably improved sensitivity, selectivity, and stability toward H_2O_2 detection.

2. Results and Discussion

During synthesis, the POMs not only serve as reducing agents for both GO and Au^{3+}, but also as bridging molecules. **Scheme 1** shows the preparation procedure for representative tricomponent Au NPs@POM–GNSs nanohybrids. The samples were centrifuged and washed with pure water before characterization. **Figure 1** shows typical transmission electron microscopy (TEM) images of the GNSs before and after decoration with Au NPs. Figure 1a displays the as-prepared graphene as a crumpled nanosheet. A typical TEM image of 39.6% Au NPs@POM–GNSs (Figure 1b) shows that Au NPs with an average diameter of 15 ± 3 nm (determined from a statistical study of 50 NPs) are uniformly dispersed on GNSs (a typical large-scaled TEM image is also shown in Figure S1, Supporting Information). It is interesting to see that the Au NPs preferentially adhere to the surfaces of GNSs, rather than to regions without GNSs. A magnified image of five Au NPs suggests an Au@POM core–shell structure for the NPs. A thin layer with about 2 nm thickness is clearly observed in Figure 1c, which is in accordance with our previous works.[28,31] The POM layer here facilitates the binding of Au NPs to the GNSs, in agreement with the earlier work demonstrating that PW12 clusters can be adsorbed on the reduced GO during the photoreduction process.[9a] The Au NPs showed a highly monocrystalline character, which is proved by the high resolution image shown in Figure 1d. The lattice fringe of Au (111) crystalline face (0.23 nm) was observed in the figure. The electrostatic repulsion between negatively charged POMs prevents Au NPs from aggregating, as was reported in our earlier work.[32] The POMs behave like an anionic stabilizer. In situ energy dispersive X-ray (EDX) analysis (Figure S2, Supporting Information) showed that strong tungsten peaks exist as well as the gold peaks, confirming the existence of the POM around Au NPs–GNSs. The strong peaks of Cu are from the copper grid. The actual Au loading of the hybrid was determined to be about 35 wt-% by inductively coupled plasma-mass spectroscopy (ICP-MS), which is close to the initial designed loading amount (39.6 wt-%).

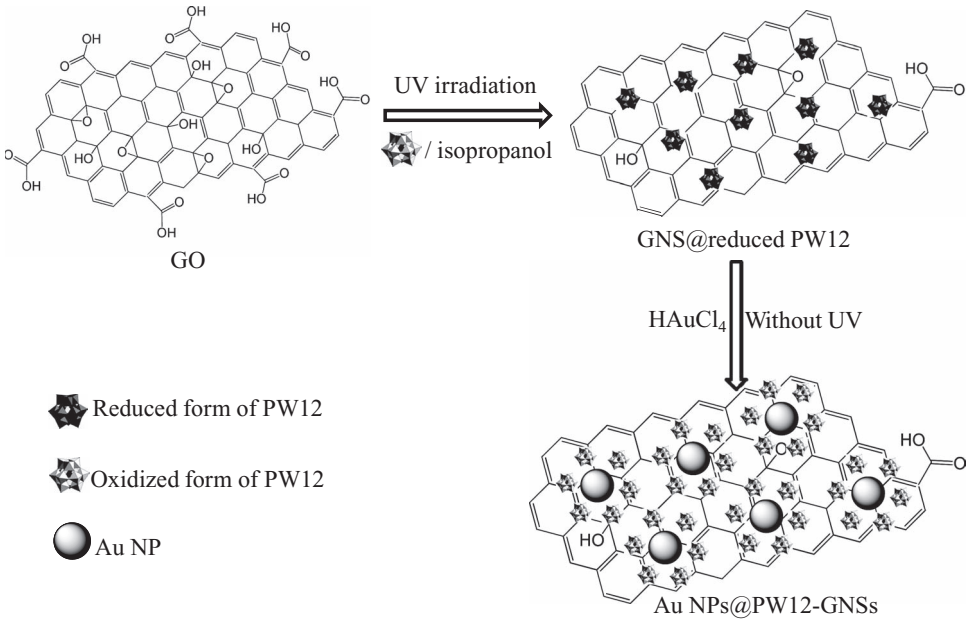

Scheme 1. Preparation procedure of representative tricomponent Au NPs@POM–GNSs nanohybrids.

The nanohybrid was further characterized by X-ray diffraction (XRD), X-ray photoelectron spectroscopy (XPS), and Raman spectroscopy. An XRD pattern of PW12, graphite (G), GO, and 39.6% Au NPs@POM–GNSs is displayed in **Figure 2**. It can be seen that G showed a sharp diffraction peak at 26.5° corresponding to (002) plane with *d*-spacing of 0.336 nm. Compared with G, the feature diffraction peak of GO appeared at 11.2° corresponding to the C (002) interlayer spacing of 0.790 nm.[33] The increase in the *d* value of GO may be due to the evolution of 0.336 nm spacing between typical graphene sheets in graphite to integrate the water molecules trapped between oxygen containing functional groups in GO sheets. The absence of any peak at a 2θ value of 26.5° reveals the complete oxidation of G.[34] After the exfoliation of GO by POM-assisted photoreduction, the sharp peak of G at 26.5° almost disappeared and became a broader peak at around 20°–30°,[35] meaning the layers of G along the *c*-axis were exfoliated and the carbon sp^2 bonds restored. In addition, the Au NPs@POM–GNSs nanohybrid also showed diffraction peaks for both the POM and Au (the observed characteristic peaks at 38.4° and 44.3° are assigned to the (111) and (200) planes of Au crystals with face-centered cubic (fcc) structure), which confirmed the formation of tricomponent hybrid of Au NPs@POM–GNSs. These results are consistent with the TEM observations.

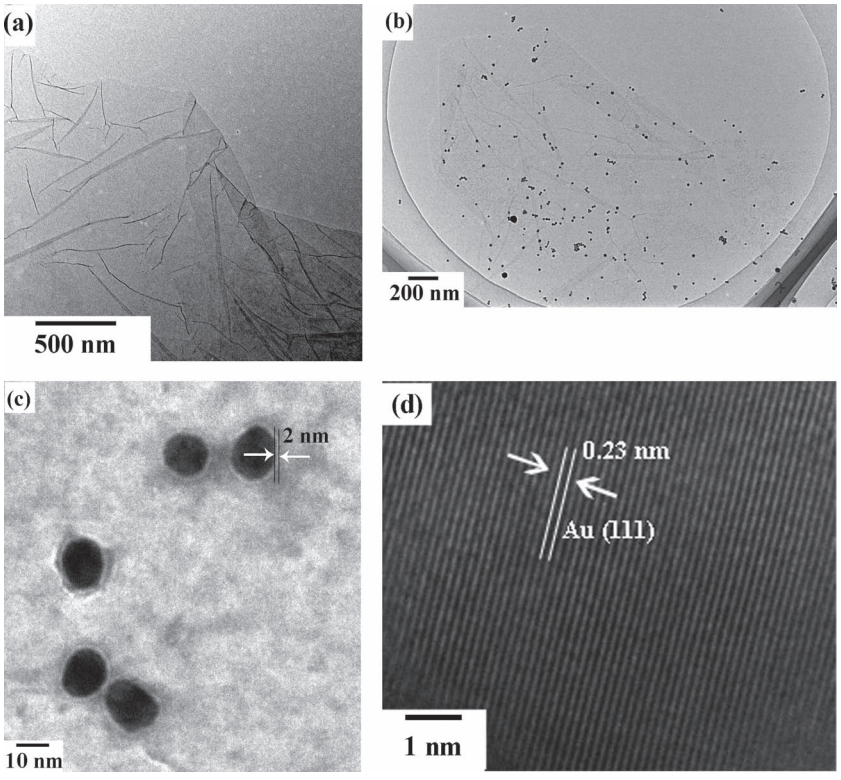

Figure 1. TEM images of: a) bare GNSs; b) 39.6% Au NPs@POM–GNSs composites; c) magnified image of five Au@POM core–shell structures; and, d) HRTEM image of single Au NP.

XPS was used to further verify the as synthesised nanohybrids. The reduction of GO was further confirmed by using XPS to detect the constitutional change of carbon atoms in different chemical states of GO before and after photoreduction. **Figure 3**a and b show the C 1*s* XPS spectra of GO and 39.6% Au NPs@POM–GNSs. As for GO (Figure 3a), four types of carbon with different chemical

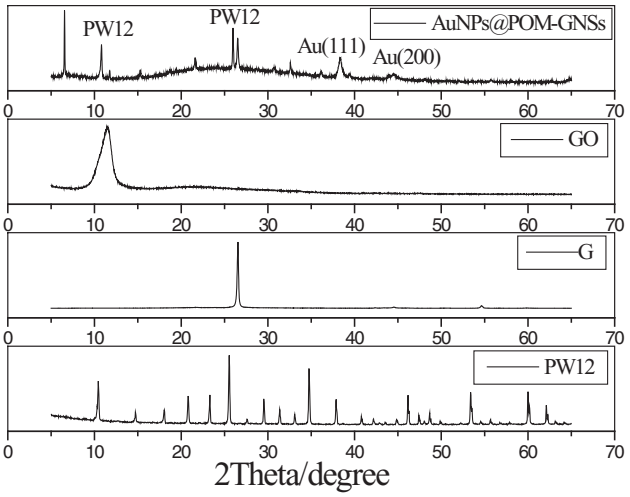

Figure 2. XRD patterns of raw PW12, natural G, GO, and the as-prepared 39.6% Au NPs@POM–GNSs.

states are observed, which appear at 284.8 eV for graphite-like C, 286.8 eV for C–O, 287.8 eV for C=O and 289.0 eV for O–C=O. After the photoreduction (Figure 3b), the content of C–O group decreases from initial 51.2% to 20.8% (shown in Table S1, Supporting Information), indicating that the photoreduction can effectively eliminate the oxygen containing groups on GO. Meanwhile, the content of C–C/C=C group increased from 39.1% to 79.0%, indicating that significant sp^3/sp^2-hybridized carbon structures were restored.

The oxidation state of gold in the NPs attached on GNSs and the presence of tungsten were also determined by XPS, as shown in Figure 3c and d. The XPS spectrum of the as-prepared Au NPs@POM–GNSs nanohybrid shows the Au 4*f* 7/2 and 4*f* 5/2 doublet (Figure 3c). With the charge effect corrected by fixing the photoelectric peak 1*s* of carbon at 284.8 eV, the 4*f* 7/2 level is located at 84.0 ± 0.3 eV and the 4*f* 5/2 level at 87.8 ± 0.3 eV.[28a] These values suggest unambiguously that gold is present only in the metallic form, indicating the formation of Au NPs on the surface of GNSs. The presence of tungsten was also detected, despite the thorough washing of the samples. As shown in Figure 3d, there are W4*f* 5/2 and W4*f* 7/2 doublets with binding energies of 36.13 and 38.23eV respectively; these values indicate that tungsten is in its full oxidation form in the POM.

Raman spectroscopy provides information on the structural properties of carboneous materials, including disorder and defect structures. The Raman spectra of the G, GO, and as-prepared 39.6% Au NPs@POM–GNSs were detected to further confirm the oxidation of G and the subsequently reduction of GO (**Figure 4**). It has been reported that the G band corresponds to the first-order scattering of the *E*2*g* mode from the sp^2 carbon domains and the D band is a breathing mode or *k*-point photons of *A*1*g* symmetry originating from the disorder-induced mode associated with structural defects and imperfections.[36] The intensity ratio of D and G bands, I_D/I_G, is a measure of disorder degree and average size of the sp^2 domains. As shown in Figure 4, G exhibited a strong sharp G band at 1564.3 cm^{-1} and a relatively weak D band at 1340.4 cm^{-1} from which I_D/I_G was 0.129. For GO, the G band broadened significantly and shifted upward to a higher frequency of 1593.2 cm^{-1}, and I_D/I_G increased to 0.949, indicating the reduction in size of the in-plane sp^2 domains due to the extensive oxidation. For the 39.6% Au NPs@POM–GNSs nanohybrids, the G band shifted back to 1580.8 cm^{-1}

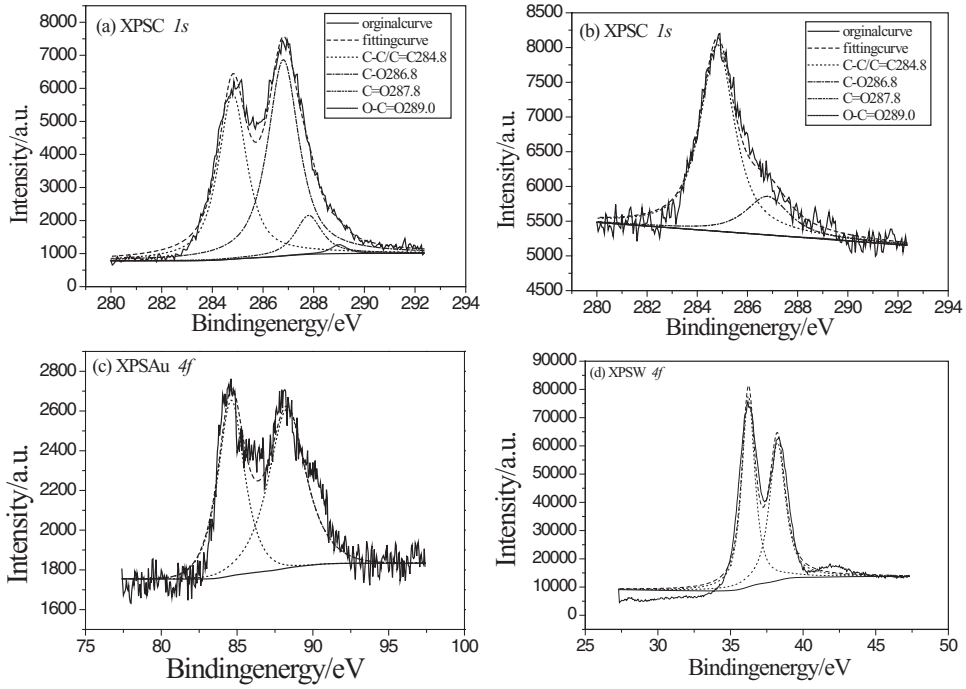

Figure 3. C 1*s* XPS spectra of: a) GO before photoreduction, and, b) as-prepared 39.6% Au NPs@POM–GNSs after photoreduction; XPS spectra of the Au 4*f* (c) and W 4*f* (d) in the as-prepared nanohybrids.

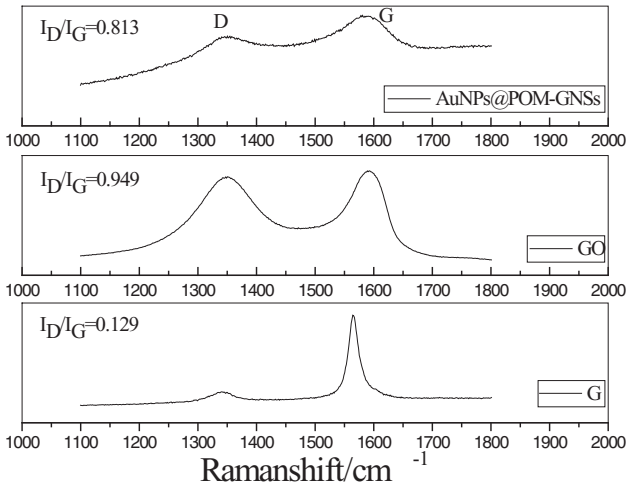

Figure 4. Raman spectra of natural G and GO before photoreduction, and as-prepared 39.6% Au NPs@POM–GNSs after photoreduction.

and I_D/I_G decreased to 0.813. Since the ratio of D/G intensity is proportional to the average size of the sp^2 domains, the PW12-assisted photoreduction indeed increased the average size of the crystalline graphene domains due to the graphitic "self-healing" in Au NPs@POM–GNSs. This is consistent with the reported results for reduced graphene by hydrazine and thermal treatment.[37,38]

The density of Au NPs on the GNSs can be simply tuned by changing the concentration of Au^{3+} under identical conditions as those used for preparation of samples in Figure 1. For example, when the concentration of $HAuCl_4$ changed from an initial 0.25 mM to 0.125 and 0.5 mM, the density of Au NPs on the surface of GNSs is substantially altered, and thus the Au loading changed to about 24.7 and 56.8 wt-%, respectively. Typical TEM images of the sample with these Au NPs loadings are shown in Figure S3 (see the Supporting Information).

The promising application as enzyme-free biosensor for H_2O_2 was selected as a preliminary test of the electrocatalytic behaviors of the prepared nanohybrids. In order to obtain the optimum potential for the amperometric measurements of the hybrids, cyclic voltammetric (CV) measurements were taken first. The CV curves of Au NPs@POM (actual Au loading mass was approximately 6.16×10^{-3} mg), hybrids of 24.7% Au NPs@POM–GNSs (actual Au loading mass was approximately 3.08×10^{-3} mg) and 39.6% Au NPs@POM–GNSs (actual Au loading mass was approximately 6.16×10^{-3} mg) electrodes in Ar-saturated 0.4 M PBS (pH = 7) toward H_2O_2 reduction are shown in **Figure 5**. According to the literature,[39–41] the mechanism for H_2O_2 electro-reduction proceeds as follows:

$$H_2O_2 + e^- \rightarrow OH_{ad} + OH^- \quad (1)$$

$$OH_{ad} + e^- \rightarrow OH^- \quad (2)$$

$$2OH^- + 2H^+ \rightarrow 2H_2O \quad (3)$$

It is clearly shown that all the catalysts exhibit catalytic activities toward H_2O_2 reduction with a cathodic reduction peak

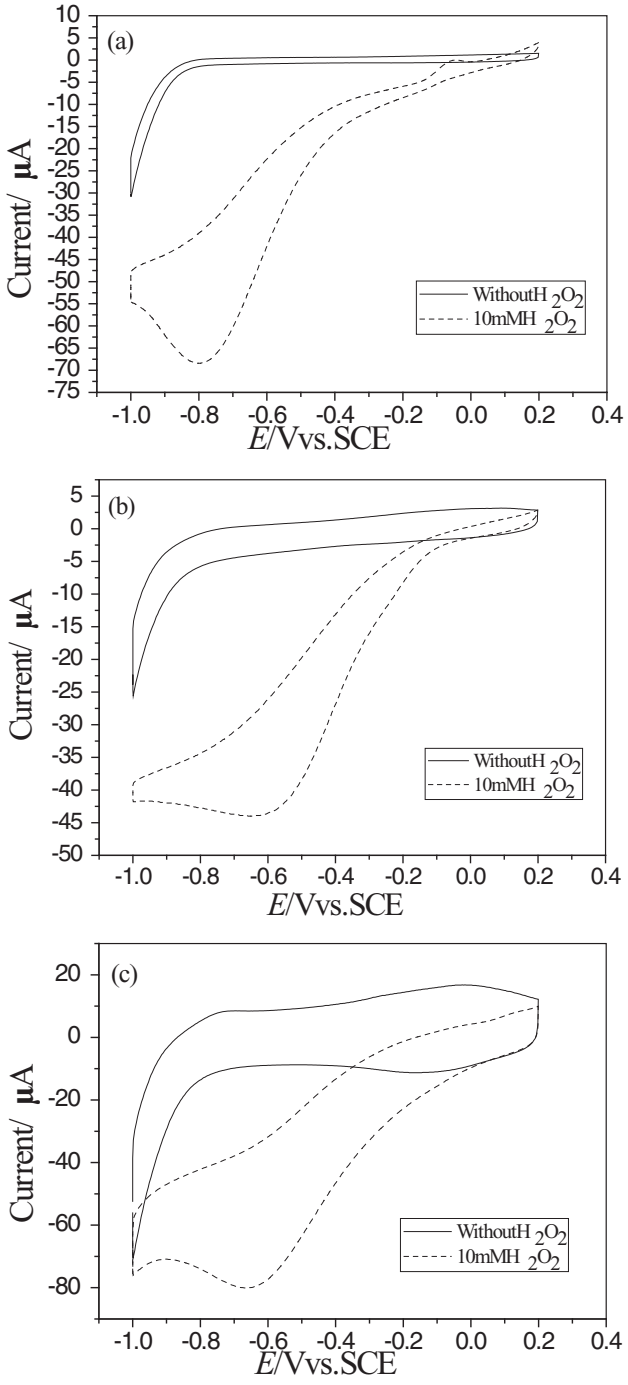

Figure 5. CV curves of Au NPs@POM (a), 24.7% Au NPs@POM–GNSs (b), and 39.6% Au NPs@POM–GNSs (c) in Ar-saturated 0.4 M PBS (pH = 7) solutions without (solid line) and with (dotted line) 10 mM H_2O_2 at a scan rate of 50 mV s^{-1}.

after addition of 10 mM H_2O_2 (dotted curves), but there was no current response without addition of H_2O_2 in the potential range –0.9 to 0.2 V vs. saturated calomel electrode (SCE) (solid curves). Compared with Au NPs@POM (Figure 5a), which showed a cathodic reduction peak at around –0.8 V vs. SCE, the peak potential of Au NPs@POM–GNSs shifted positively to –0.65 V vs. SCE. (Figure 5b and c) with a higher peak current response, indicating a higher electrocatalytic

NANO MICRO small

activity of the synthesized Au NPs@POM–GNSs nanohybrids towards H_2O_2 reduction than the Au NPs@POM. We attribute the better performance of the nanohybrids to the following two major factors: i) the highly conductive GNSs connect gold nanoparticles and improve the charge transfer between the modifying layer and substrate glassy carbon (GC) electrode; and, ii) a synergistic effect of the well-dispersed Au NPs and GNSs is beneficial to their electrocatalytic activities.

As shown above, the as-prepared Au NPs@POM–GNSs nanohybrids displayed higher catalytic activities than the Au NPs@POM electrode. Thus the amperometric response to H_2O_2 of the Au NPs@POM–GNSs was studied to make sure that the as-prepared nanohybrids possess promise for application as enzyme-free biosensors. There is no doubt that the sensitivity of electrochemical biosensors is strongly dependent on the applied potential. The cathodic current of H_2O_2 obtained at Au NPs@POM–GNSs nanohybrid-modified electrodes increased with the negative shift of the operating potentials and reached a highest current at about –0.65 V vs. SCE. So the electrode potential –0.65 V vs. SCE was selected as the optimized potential after an overall consideration of the detection sensitivity, where the background current is minimized. Under these optimum conditions, a typical current–time plot of 39.6% Au NPs@POM–GNSs modified electrode upon the successive addition of aliquots of H_2O_2 is shown in **Figure 6**a. As the H_2O_2 was added into the stirred PBS solution, well-defined steady-state current responses were obtained in around 3 s at the applied potential, and the currents increased stepwise with successive additions of H_2O_2. It can be concluded that small molecules have a rapid diffusion from the solution to the nanohybrids modified electrode and that the better electron transfer rate of GNSs may play an important role. Moreover, the obvious increase of the current could be observed when the concentration of H_2O_2 was as low as 5 μM (Figure 6b, a local image corresponding to the rectangular area of Figure 6a shown for the response of the low concentrations of H_2O_2). The corresponding calibration curve shown in Figure 6c indicated that the hydrogen peroxide biosensor based on 39.6% Au NPs@POM–GNSs exhibited a linear response range (LRR) from 5×10^{-6} to 1.8×10^{-2} M with a linear regression equation (LRE) of I (μA) = 4.12 C (mM) – 0.18 (R = 0.99979), a limit of detection (LOD) of 1.54 μM (based on S/N = 3) and a sensitivity of 58.87 μA cm^{-2} mM^{-1}. Figure 6d is a local image corresponding to the rectangular area of Figure 6c. When we further studied the performance of the as-prepared hybrids in details, it is interesting to find that the sensitivity of the hybrids can be tuned by the actual Au loading mass in the hybrids; the resulting performance of the 24.7% and 56.8% Au NPs@POM–GNSs (actual Au loading mass was approximately 1.23×10^{-2} mg) were is shown in Figure S4 and S5 (see Supporting Information), respectively. Encouragingly, a lower LOD of 1.33 μM was obtained from 56.8% Au NPs@POM–GNSs. Table S2 (see Supporting Information) is shown for a visualized comparison of the performance for different Au NPs@POM–GNSs nanohybrids to H_2O_2 detection. It can be seen that the sensitivity of the nanohybrid becomes higher with increasing Au loading.

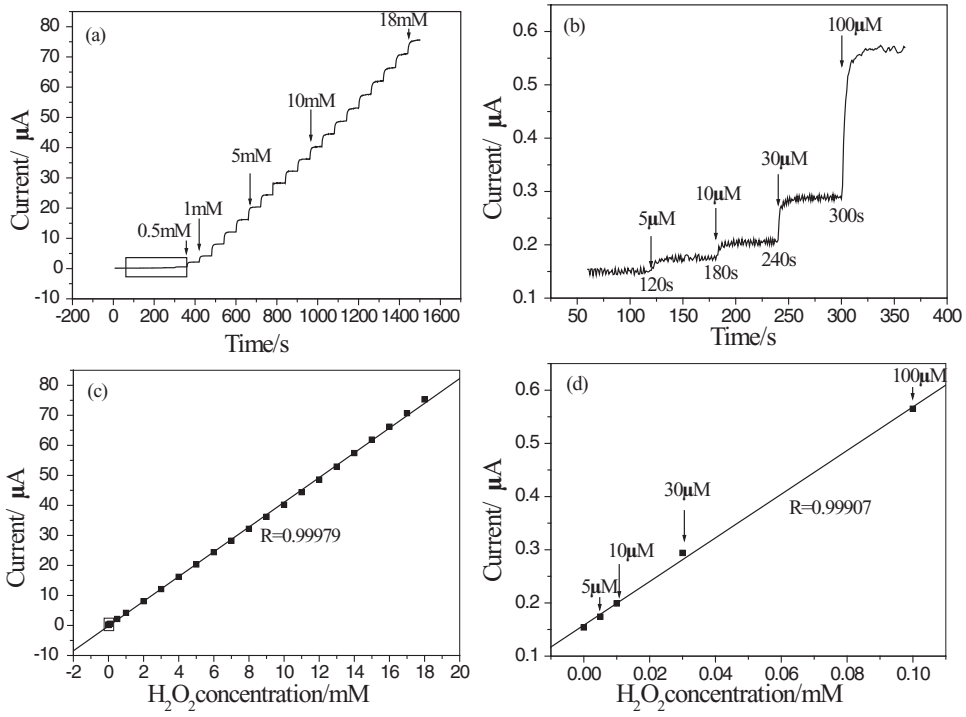

Figure 6. Typical amperometric responses of the 39.6% Au NPs@POM–GNSs modified electrode to successive addition of aliquot H_2O_2 at –0.65 V vs.SCE in 0.4 M PBS solution (pH = 7.0) (a) and the corresponding calibration plot of steady-state currents against concentrations of H_2O_2 (c). (b) and (d) are local images corresponding to the rectangular area of (a) and (c), respectively.

The H_2O_2 detection performance of the proposed biosensor was compared with other biosensors based on Au NPs; the results are shown in Table S3 (see Supporting Information). They show that the Au NPs@POM–GNSs exhibits excellent performance in terms of a wider LRR, a relatively lower LOD, and fast current response for H_2O_2, suggesting the proposed biosensor based on Au NPs@POM–GNSs nanohybrids can be compared advantageously with respect to other Au-based enzymatic and non-enzymatic biosensor designs. The graphene here plays an extremely positive role, as was shown in our previous work in which the Au NPs@POM system had a relatively narrow LRR from 5×10^{-6} to 1.0×10^{-2} M toward H_2O_2 detection.[42]

Since selectivity and stability are two important factors in the performance of a biosensor, we investigated the selectivity and stability of 39.6% Au NPs@POM–GNSs-based H_2O_2 biosensor in details. Several common electroactive compounds in real biological samples – ethanol, methanol, glucose, and ascorbic acid – were measured to examine whether they interfered with the determination of H_2O_2. As shown in Figure S6 (see Supporting Information), H_2O_2 solution was first injected into the electrochemical cell, followed by the addition of interferents. It can be observed that an obvious amperometric response appeared immediately when 0.1 mM H_2O_2 was injected at 120 s. However, the subsequent addition of ethanol (1 mM), methanol (1 mM), glucose (0.5 mM). and ascorbic acid (0.2 mM) did not cause any further amperometric changes. When more H_2O_2 was added to reach 0.5 mM, the current changed proportionally even with the existence of the interferents, indicating the nanohybrid has a good selectivity to H_2O_2.

The electrode was stored in air at room temperature when not in use. The stability of the biosensor under storage was investigated by measuring the amperometric response in 0.4 M PBS (pH = 7) under successive addition of aliquots of H_2O_2 after 1 week. It can be observed that the biosensor still had the high sensitivity to H_2O_2 detection and had almost 99% of its original current response to H_2O_2 (**Figure 7**). The good long-term stability could be attributed to the strong interaction between Au NPs and GNSs.

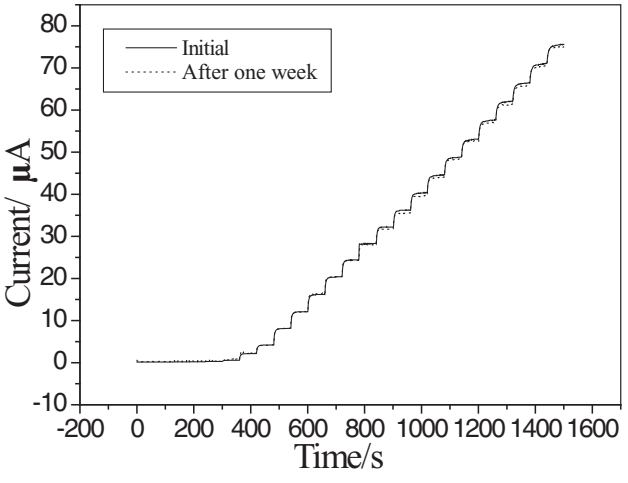

Figure 7. Amperometric responses of the 39.6% Au NPs@POM–GNSs-modified electrode to successive addition of aliquots of H_2O_2 at −0.65 V vs.SCE in 0.4 M PBS solution (pH = 7.0) at initial test (solid line) and tested after 1 week (dotted line).

It should be noted that the present POM is not stable in the proposed experimental environment (pH = 7), as was suggested in our previous work[28][c] and also elsewhere.[43a] Thus, the corresponding fragments issued from the decomposition may remain in the hybrids during the electrochemical reactions. This was confirmed by the CV characteristics of PW12 before and after the experiment of H_2O_2 detection (Figure S7, see Supporting Information). Both the characteristic features of bulk gold electrodes (0.9 V vs. SCE) and the POM redox systems (1 electron reduction peak of PW12 at –0.02 V vs. SCE)[43b,c] before H_2O_2 detection were observed. While the POM redox systems disappeared after H_2O_2 detection, which indicated the decomposition of the PW12. However, such decomposition of the POMs does not affect the catalytic activities of the nanohybrid, as shown in the stability test. GNSs and Au NPs are known to promote fast electron transport within their structures. As a consequence, it can be hypothesized that the superior catalytic activities of the nanohybrids toward H_2O_2 may be mostly attributed to a synergistic effect of Au NPs and GNSs, reinforced by the presence of decomposition fragments of the POM.

3. Conclusion

Novel tricomponents of Au NPs@POM–GNSs were prepared using solely POM as both reducing, encapsulating molecules and bridging molecules. This synthesis is green, simple, and rapid. The Au NPs@POM–GNSs nanohybrids showed high electrocatalytic activity towards H_2O_2 reduction because of the synergistic effect of Au NPs and GNSs. The Au NPs@POM–GNSs nanohybrids have high catalytic activity with good sensitivity, good long-term stability, wide linear range, low detection limit, and fast response towards H_2O_2 detection for application as enzyme-free biosensors. This unique nanohybrid material has wide potential applications in biosensors and catalysis. At the same time, the methodology developed in this study could serve as a general approach to the development of other metal NPs@POM–GNSs nanohybrids that also have potentially catalytic activities.

4. Experimental Section

Materials: PW12 and $HAuCl_4 \cdot 3H_2O$ were purchased from the Aldrich Chemical Company. Isopropanol was purchased from the Beijing Chemical Reagents Corporation (Analytic grade) and was used as received. All other reagents were of analytical grade. Ultrapure water purified with the Milli-Q (MQ) plus system (Millipore Co.) with resistivity of 18.2 MΩ cm was used exclusively in all aqueous solutions and rinsing procedures.

Synthesis of Nanohybrid of Au NPs@POM–GNSs: GO was oxidized from natural G flakes by a modified Hummers' method[44] using H_2SO_4, $NaNO_3$, and $KMnO_4$ in an ice bath, as reported in great detail elsewhere.[9] The resulting homogeneous brown GO dispersion was tested to be stable over several months and used for reduction. For preparation of Au NPs@POM–GNSs nanohybrid, the PW12 was first reduced photochemically. A 500 W Hg lamp

NANO MICRO small

was used as a UV light source. In a typical synthesis, PW12 (2 mL, 2 mM) was added in a spectrophotometer cell (1 cm pathlength) and mixed with isopropanol (220 μL). GO (19 μL, 8 mg mL^{-1}) was then added into the mixed solution followed by deaeration with Ar for 15 min. Then the mixed solution was irradiated under UV light for 30 min. The concentration of the reduced PW12 can be controlled by varying the irradiation time. Then the blue–black solution of reduced PW12 and GNSs hybrids was mixed with aqueous solution of $HAuCl_4$ (1 μL, 0.5 M) at room temperature by soft shaking by hand. After several minutes of reaction, the tricomponent nanohybrids were prepared. The samples were then centrifuged at 13 500 rpm for 60 min and washed three times with pure water. At last, the samples were redispersed in pure water (2 mL). The Au NPs@POM was prepared by the same method, without adding GO.

Characterization: TEM images were obtained using a JEM-2010 transmission electron microscope at an acceleration voltage of 200 kV. XPS measurements were performed in ultrahigh vacuum (UHV) with Krato, AXIS-HS monochromatized Al Kα cathode source, at 75–150 W, using a low-energy electron gun for charge neutralization. XRD studies were recorded on a Bruker AXS D advance powder diffractometer with a Cu Kα (λ = 0.15418 nm) source. Raman spectra were obtained with a Renishaw Raman system model 1000 spectrometer. The 532 nm radiation from a 20 mW air-cooled argon ion laser was used as the exciting source. The laser diameter was 1 μm, and the laser power at the sample position was 4.0 mW. The data acquisition time was 10 s. The composition of catalysts was determined by ICP-MS (X Series 2, Thermo Scientific USA).

Electrochemistry Experiments: The mother solution was centrifuged at 13 500 rpm for 60 min and partial black catalyst paste (approximately 80 μL) was left in the bottom of the centrifuge tube. Then, the prepared catalyst ink (5 μL) was dropped onto the surface of a pre-polished GC disk electrode (3 mm in diameter), followed by dropping Nafion solution (0.5%, 5 μL) in isopropanol as a binder after 12 h.

CV and amperometric measurements were performed on a ZAHNER ZENNIUM electrochemical workstation (ZAHNER Instrument, Inc.). A standard three-electrode cell was used and was controlled at 25 °C using a water bath during the experiment. A platinum foil (3.0 cm^2) and SCE were used as counter and reference electrode, respectively. The prepared thin-film GC electrode was used as the working electrode. The electrolyte, consisting of a solution of 0.5 M H_2SO_4 or 0.4 M phosphate buffer solution (PBS, pH 7.0), was saturated with ultrahigh-purity Ar for 30 min before CV measurements and an Ar atmosphere was kept over the solution in the cell during amperometric measurements. In steady-state amperometric experiments, the potential was set at –0.65 V with a stirring rate of 300 rpm, and the current–time curves were recorded after a constant background current had been established.

Supporting Information

Supporting Information is available from the Wiley Online Library or from the author.

Acknowledgements

This work was supported by the One Hundred Talent Program of the Institute of Process Engineering, Chinese Academy of Sciences, National Natural Science Foundation of China (No. 21071146, 51002155) and by the University Paris-Sud 11 (UMR 8000, CNRS), France.

[1] K. S. Novoselov, A. K. Geim, S. V. Morozov, D. Jiang, Y. Zhang, S. V. Dubonos, I. V. Grigorieva, A. A. Firsov, *Science* **2004**, *306*, 666.
[2] M. D. Stoller, S. J. Park, Y. W. Zhu, J. H. An, R. S. Ruoff, *Nano Lett.* **2008**, *8*, 3498.
[3] A. K. Geim, *Science* **2009**, *324*, 1530.
[4] K. S. Novoselov, A. K. Geim, S. V. Morozov, D. Jiang, M. I. Katsnelson, I. V. Grigorieva, S. V. Dubonos, A. A. Firsov, *Nature* **2005**, *438*, 197.
[5] Y. B. Zhang, Y. W. Tan, H. L. Stormer, P. Kim, *Nature* **2005**, *438*, 201.
[6] S. Stankovich, D. A. Dikin, G. H. B. Dommett, K. M. Kohlhaas, E. J. Zimney, E. A. Stach, R. D. Piner, S. T. Nguyen, R. S. Ruoff, *Nature* **2006**, *442*, 282.
[7] J. S. Bunch, A. M. van der Zande, S. S. Verbridge, I. W. Frank, D. M. Tanenbaum, J. M. Parpia, H. G. Craighead, P. L. McEuen, *Science* **2007**, *315*, 490.
[8] C. Xu, X. Wang, J. W. Zhu, *J. Phys. Chem. C* **2008**, *112*, 19841.
[9] a) H. L. Li, S. P. Pang, X. L. Feng, K. Müllen, C. Bubeck, *Chem. Commun.* **2010**, *46*, 6243; b) H. L. Li, S. P. Pang, S. Wu, X. L. Feng, K. Müllen, C. Bubeck, *J. Am. Chem. Soc.* **2011**, *133*, 9423.
[10] C. Stampfer, E. Schurtenberger, F. Molitor, J. Guttinger, T. Ihn, K. Ensslin, *Nano Lett.* **2008**, *8*, 2378.
[11] E. Yoo, J. Kim, E. Hosono, H. S. Zhou, T. Kudo, I. Homa, *Nano Lett.* **2008**, *8*, 2277.
[12] Z. Y. Yin, S. Y. Sun, T. Salim, S. X. Wu, X. Huang, Q. Y. He, Y. M. Lam, H. Zhang, *ACS Nano* **2010**, *4*, 5263.
[13] Y. Sui, J. Appenzeller, *Nano Lett.* **2009**, *9*, 2973.
[14] X. Wu, Y. Hu, J. Jin, N. Zhou, P. Wu, C. X. Cai, *Anal. Chem.* **2010**, *82*, 3588.
[15] J. Lu, L. T. Drzal, R. M. Worden, I. Lee, *Chem. Mater.* **2007**, *19*, 6240.
[16] P. D. Cozzoli, T. Pellegrino, L. Manna, *Chem. Soc. Rev.* **2006**, *35*, 1195, and references therein.
[17] X. Huang, X. Y. Qi, F. Boey, H. Zhang, *Chem. Soc. Rev.* **2012**, *41*, 666, and references therein.
[18] S. J. Guo, D. Wen, Y. M. Zhai, S. J. Dong, E. Wang, *ACS Nano* **2010**, *4*, 3959.
[19] K. Vinodgopal, B. Neppolian, I. V. Lightcap, F. Grieser, M. Ashokkumar, P. V. Kamat, *J. Phys. Chem. Lett.* **2010**, *1*, 1987.
[20] Y. J. Hu, J. Jin, P. Wu, H. Zhang, C. X. Cai, *Electrochim. Acta* **2010**, *56*, 491.
[21] F. A. He, J. T. Fan, F. Song, L. M. Zhang, H. L. W. Chan, *Nanoscale* **2011**, *3*, 1182.
[22] a) K. F. Zhou, Y. H. Zhu, X. L. Yang, C. Z. Li, *Electroanal.* **2010**, *22*, 259; b) K. F. Zhou, Y. H. Zhu, X. L. Yang, C. Z. Li, S. R. Luan, *Electrochim. Acta* **2010**, *55*, 3055.
[23] T. T. Baby, S. S. Jyothirmayee Aravind, T. Arockiadoss, R. B. Rakhi, S. Ramaprabhu, *Sens. Actuators, B:* **2010**, *145*, 71.
[24] Y. Wang, S. Zhang, D. Du, Y. Y. Shao, Z. H. Li, J. Wang, M. H. Engelhard, J. H. Li, Y. H. Lin, *J. Mater. Chem.* **2011**, *21*, 5319.
[25] M. H. Yang, B. G. Choi, H. Park, T. J. Park, W. H. Hong, S. Y. Lee, *Electroanalysis* **2011**, *23*, 850.
[26] J. M. Gong, X. J. Miao, T. Zhou, L. Z. Zhang, *Talanta* **2011**, *85*, 1344.
[27] K. Kriz, M. Anderlund, D. Kriz, *Biosens. Bioelectron.* **2001**, *16*, 363.

[28] a) S. W. Li, X. L. Yu, G. J. Zhang, Y. Ma, J. N. Yao, B. Keita, L. Nadjo, H. Zhao, *J. Mater. Chem.* **2011**, *21*, 2282; b) S. W. Li, X. L. Yu, G. J. Zhang, Y. Ma, J. N. Yao, P. Oliveira, *Carbon* **2011**, *49*, 1906; c) R. J. Liu, S. W. Li, X. L. Yu, G. J. Zhang, Y. Ma, J. N. Yao, *J. Mater. Chem.* **2011**, *21*, 14917.
[29] C. L. Hill, D. A. Bouchard, *J. Am. Chem. Soc.* **1985**, *107*, 5148.
[30] A. Troupis, A. Hiskia, E. Papaconstantinou, *Angew. Chem., Int. Ed.* **2002**, *41*, 1911.
[31] G. J. Zhang, B. Keita, A. Dolbecq, P. Mialane, F. Sécheresse, F. Miserque, L. Nadjo, *Chem. Mater.* **2007**, *19*, 5821.
[32] R. J. Liu, S. W. Li, X. L. Yu, G. J. Zhang, Y. Ma, J. N. Yao, B. Keita, L. Nadjo, *Cryst. Growth Des.* **2011**, *11*, 3424.
[33] S. Zhang, Y. Y. Shao, H. G. Liao, M. H. Engelhard, G. P. Yin, Y. H. Lin, *ACS Nano* **2011**, *5*, 1785.
[34] Y. X. Xu, H. Bai, G. W. Lu, C. Li, G. Q. Shi, *J. Am. Chem. Soc.* **2008**, *130*, 5856.
[35] G. H. Jeong, S. H. Kim, M. Kim, D. Choi, J. H. Lee, J. Kim, S. Kim, *Chem. Commun.* **2011**, *47*, 12236.
[36] A. C. Ferrari, J. C. Meyer, V. C. Scardaci, C. M. Lazzeri, F. Mauri, S. Piscanec, D. Jiang, K. S. Novoselov, S. Roth, A. K. Geim, *Phys. Rev. Lett.* **2006**, *97*, 187401.
[37] K. N. Kudin, B. Ozbas, H. C. Schniepp, R. K. Prud'homme, I. A. Aksay, R. Car, *Nano Lett.* **2008**, *8*, 36.
[38] A. Reina, X. T. Jia, J. Ho, D. Nezich, H. B. Son, V. Bulovic, M. S. Dresselhaus, J. Kong, *Nano Lett.* **2009**, *9*, 30.
[39] F. H. Meng, X. L. Yan, J. G. Liu, J. Gu, Z. G. Zou, *Electrochim. Acta* **2011**, *56*, 4657.
[40] T. G. J. Van Venrooij, M. T. M. Koper, *Electrochim. Acta* **1995**, *40*, 1689.
[41] G. Flatgen, S. Wasle, M. Lubke, C. Eickes, G. Radhakrishnan, K. Doblhofer, G. Ertl, *Electrochim. Acta* **1999**, *44*, 4499.
[42] G. J. Zhang, B. Keita, R. N. Biboum, F. Miserque, P. Berthet, A. Dolbecq, P. Mialane, L. Catala, L. Nadjo, *J. Mater. Chem.* **2009**, *19*, 8639.
[43] a) B. Keita, D. Bouaziz, L. Nadjo, *Electroanalysis* **1991**, *3*, 637; b) B. Keita, L. Nadjo, *J. Electroanal. Chem.* **1985**, *191*, 441; c) B. Keita, L. Nadjo, *J. Electroanal. Chem.* **1987**, *217*, 287.
[44] W. S. Hummers, R. E. Offeman, *J. Am. Chem. Soc.* **1958**, *80*, 1339.

Received: October 31, 2011
Published online: February 21, 2012

